

# DETECTION OF GRB 060927 AT $z = 5.47$ : IMPLICATIONS FOR THE USE OF GAMMA-RAY BURSTS AS PROBES OF THE END OF THE DARK AGES<sup>1</sup>

A. E. RUIZ-VELASCO<sup>2,3</sup>, H. SWAN<sup>4</sup>, E. TROJA<sup>5,6,7</sup>, D. MALESANI<sup>2</sup>, J. P. U. FYNBO<sup>2</sup>, R. L. C. STARLING<sup>5</sup>, D. XU<sup>2</sup>, F. AHARONIAN<sup>8</sup>, C. AKERLOF<sup>4</sup>, M. I. ANDERSEN<sup>9</sup>, M. C. B. ASHLEY<sup>10</sup>, S. D. BARTHELMEY<sup>11</sup>, D. BERSIER<sup>12</sup>, J. M. CASTRO CERÓN<sup>2</sup>, A. J. CASTRO-TIRADO<sup>13</sup>, N. GEHRELS<sup>11</sup>, E. GÖĞÜŞ<sup>14</sup>, J. GOROSABEL<sup>13</sup>, C. GUIDORZI<sup>12,15</sup>, T. GÜVER<sup>16</sup>, J. HJORTH<sup>2</sup>, D. HORNS<sup>8</sup>, K. Y. HUANG<sup>17</sup>, P. JAKOBSSON<sup>18</sup>, B. L. JENSEN<sup>2</sup>, Ü. KIZILOĞLU<sup>19</sup>, C. KOUVELIOTOU<sup>20</sup>, H. A. KRIMM<sup>11,21</sup>, C. LEDOUX<sup>22</sup>, A. J. LEVAN<sup>23</sup>, T. MARSH<sup>23</sup>, T. MCKAY<sup>4</sup>, A. MELANDRI<sup>12</sup>, B. MILVANG-JENSEN<sup>2</sup>, C. G. MUNDELL<sup>12</sup>, P. T. O'BRIEN<sup>5</sup>, M. ÖZEL<sup>24</sup>, A. PHILLIPS<sup>10</sup>, R. QUIMBY<sup>25</sup>, G. ROWELL<sup>8</sup>, W. RUJOPAKARN<sup>26</sup>, E. S. RYKOFF<sup>4</sup>, B. E. SCHAEFER<sup>27</sup>, J. SOLLERMAN<sup>2</sup>, N. R. TANVIR<sup>5</sup>, C. C. THONE<sup>2</sup>, Y. URATA<sup>28</sup>, W. T. VESTRAND<sup>29</sup>, P. M. VREESWIJK<sup>22</sup>, D. WATSON<sup>2</sup>, J. C. WHEELER<sup>25</sup>, R. A. M. J. WIJERS<sup>30</sup>, J. WREN<sup>29</sup>, S. A. YOST<sup>4</sup>, F. YUAN<sup>4</sup>, M. ZHAI<sup>31</sup> AND W. K. ZHENG<sup>31</sup>.

*Draft version February 1, 2008*

## ABSTRACT

We report on follow-up observations of the gamma-ray burst GRB 060927 using the robotic ROTSE-IIIa telescope and a suite of larger aperture ground-based telescopes. An optical afterglow was detected 20 s after the burst, the earliest rest-frame detection of optical emission from any GRB. Spectroscopy performed with the VLT about 13 hours after the trigger shows a continuum break at  $\lambda \approx 8070$  Å, produced by neutral hydrogen absorption at  $z \approx 5.6$ . We also detect an absorption line at 8158 Å which we interpret as Si II  $\lambda$  1260 at  $z = 5.467$ . Hence, GRB 060927 is the second most distant GRB with a spectroscopically measured redshift. The shape of the red wing of the spectral break can be fitted by a damped Ly $\alpha$  profile with a column density with  $\log(N_{\text{HI}}/\text{cm}^{-2}) = 22.50 \pm 0.15$ . We discuss the implications of this work for the use of GRBs as probes of the end of the dark ages and draw three main conclusions: *i*) GRB afterglows originating from  $z \gtrsim 6$  should be relatively easy to detect from the ground, but rapid near-infrared monitoring is necessary to ensure that they are found; *ii*) The presence of large H I column densities in some GRBs host galaxies at  $z > 5$  makes the use of GRBs to probe the reionization epoch via spectroscopy of the red damping wing challenging; *iii*) GRBs appear crucial to locate typical star-forming galaxies at  $z > 5$  and therefore the type of galaxies responsible for the reionization of the universe.

*Subject headings:* gamma rays: bursts (GRB 060927) — cosmology

## 1. INTRODUCTION

It is well established that most long-duration gamma-ray bursts (GRBs) are caused by the death of massive stars (e.g. Galama et al. 1998; Hjorth et al. 2003;

<sup>1</sup> Partly based on observations carried out with the ESO telescopes under programmes 077.D-0661, 077.A-0667, 078.D-0416, and the large programme 177.A-f0591.

<sup>2</sup> Dark Cosmology Centre, Niels Bohr Institute, University of Copenhagen, Juliane Maries Vej 30, 2100 Copenhagen, Denmark

<sup>3</sup> Departamento de Astronomía, Universidad de Guanajuato, Apartado Postal 144, 36000 Guanajuato, Mexico

<sup>4</sup> University of Michigan, 2477 Randall Laboratory, 450 Church St., Ann Arbor, MI, 48109, USA

<sup>5</sup> Department of Physics and Astronomy, University of Leicester, University Road, Leicester LE1 7RH, UK

<sup>6</sup> INAF-Istituto di Astrofisica Spaziale e Fisica Cosmica Sezione di Palermo, Via Ugo La Malfa 153, 90146 Palermo, Italy

<sup>7</sup> Dipartimento di Scienze Fisiche ed Astronomiche, Sezione di Astronomia, Università di Palermo, Piazza del Parlamento 1, 90134 Palermo, Italy

<sup>8</sup> Max-Planck-Institut für Kernphysik, Saupfercheckweg 1, 69117 Heidelberg, Germany

<sup>9</sup> Astrophysikalisches Institut, 14482 Potsdam, Germany

<sup>10</sup> School of Physics, Department of Astrophysics and Optics, University of New South Wales, Sydney, NSW 2052, Australia

<sup>11</sup> NASA/Goddard Space Flight Center, Greenbelt, MD 20771, USA

<sup>12</sup> Astrophysics Research Institute, Liverpool John Moores University, Twelve Quays House, Egerton Wharf, Birkenhead CH41 1LD, UK

<sup>13</sup> Instituto de Astrofísica de Andalucía (IAA-CSIC), Apartado de Correos, 3.004, E-18.080 Granada, Spain

<sup>14</sup> Sabancı University, Orhanlı-Tuzla 34956 Istanbul, Turkey

<sup>15</sup> INAF-Osservatorio Astronomico di Brera, via Bianchi 46, 23807, Merate, Italy

<sup>16</sup> Istanbul University, Science Faculty Department of Astronomy & Space Sciences, Istanbul 34119, Turkey

<sup>17</sup> Institute of Astronomy, National Central University, Ching-Li

32054, Taiwan

<sup>18</sup> Centre for Astrophysics Research, University of Hertfordshire, College Lane, Hatfield, Herts AL10 9AB, UK

<sup>19</sup> Middle East Technical University, 06531 Ankara, Turkey

<sup>20</sup> NASA Marshall Space Flight Center, NSSTC, VP-62, 320 Sparkman Drive, Huntsville, AL 35805, USA

<sup>21</sup> Universities Space Research Association, 10211 Wincopan Circle, Suite 500, Columbia, MD 21044, USA

<sup>22</sup> European Southern Observatory, Alonso de Córdova 3107, Casilla 19001, Vitacura, Santiago 19, Chile

<sup>23</sup> Department of Physics, University of Warwick, Coventry, CV4 7AL, UK

<sup>24</sup> Çanakkale Onsekiz Mart Üniversitesi, Terzioğlu 17020, Çanakkale, Turkey

<sup>25</sup> Department of Astronomy, University of Texas, Austin, TX 78712, USA

<sup>26</sup> Steward Observatory, University of Arizona, Tucson, AZ 85721, USA

<sup>27</sup> Department of Physics and Astronomy, Louisiana State University, Baton Rouge Louisiana 70803, USA

<sup>28</sup> Department of Physics, Saitama University, Shimo-Okubo, Sakura, Saitama 338-8570, Japan

<sup>29</sup> Los Alamos National Laboratory, NIS-2 MS D436, Los Alamos, NM 87545, USA

<sup>30</sup> Institute of Astronomy “Anton Pannekoek”, University of Amsterdam, Kruislaan 403, 1098 SJ Amsterdam, The Netherlands

<sup>31</sup> National Astronomical Observatories, Chinese Academy of Sciences, Beijing 100012, China

Stanek et al. 2003) and, due to their brightness, they can be seen throughout the observable universe (Kawai et al. 2006). Given these facts, it has long been realized that GRBs could be powerful probes of star-formation activity throughout the history of the universe (e.g. Wijers et al. 1998). The currently operating *Swift* satellite (Gehrels et al. 2004) has revolutionized the GRB field: it has not only increased the detection rate of rapidly well-localized GRBs by roughly an order of magnitude compared to previous missions, but it also detects much fainter and more distant bursts (Jakobsson et al. 2006a). In the *Swift* era, GRBs have indeed become cosmological probes of the early Universe, as already extensively predicted in the literature (e.g. Wijers et al. 1998; Lamb & Reichart 2000). In particular, Barkana & Loeb (2004) argue that GRBs may be optimal probes of the epoch of reionization.

Here we present observations of GRB 060927 for which we determine a very high redshift ( $z = 5.467$ , § 2.3). In § 3 we discuss the light curve and the properties of the afterglow in the context of the fireball model. In § 4 we end by revisiting the question of how GRBs may be used to probe the end of the dark ages.

Throughout this paper we assume a cosmology with  $H_0 = 70 \text{ km s}^{-1} \text{ Mpc}^{-1}$ ,  $\Omega_m = 0.3$  and  $\Omega_\Lambda = 0.7$ . In this model, a redshift of 5.47 corresponds to a luminosity distance  $D_{\text{lum}} = 51.9 \text{ Gpc}$  and a distance modulus  $\mu = 48.6 \text{ mag}$ . At that distance,  $1''$  on the sky corresponds to 6.01 proper kpc and the look-back time is 12.4 Gyr (roughly 92% of the time since the Big Bang).

## 2. OBSERVATIONS AND DATA ANALYSIS

### 2.1. High-Energy Properties

GRB 060927 and its X-ray afterglow were detected by the Burst Alert Telescope (BAT) and the X-ray Telescope (XRT) on-board the *Swift* spacecraft on 2006 September 27.58860 UT. At the measured redshift of  $z = 5.47$  (§ 2.3) the BAT 15–150 keV energy band and the XRT 0.3–10 keV energy band correspond to 97–970 keV and 1.9–64.7 keV in the source rest frame, respectively. Here we describe the burst phenomenology as observed by the *Swift* instruments. Data have been analyzed using the standard analysis software distributed within FTOOLS<sup>32</sup> v. 6.1.1.

The gamma-ray prompt emission shows a complex light curve with an initial bright episode, split into two peaks. The peak flux is reached during the first peak,  $\sim 0.7 \text{ s}$  after the trigger ( $T_0$ ), and the emission subsequently decays to the background level at  $\sim T_0 + 9 \text{ s}$ . A fainter bump is visible at  $\sim T_0 + 20 \text{ s}$ . The observed duration is  $T_{90} = 22.6 \pm 0.3 \text{ s}$ , which, accounting for the  $(1+z)$  time stretching factor, corresponds to  $3.54 \pm 0.05 \text{ s}$  in the source rest frame. GRB 060927 is thus a long-duration GRB (Kouveliotou et al. 1993), both in the observer's frame and in the rest frame.

A simple power-law model is not a good fit to the BAT time-average spectrum of the burst ( $\chi^2 = 72$  for 57 d.o.f.). A significant improvement is achieved by adopting a cutoff power law ( $\chi^2 = 58$  for 56 d.o.f.), which provides a photon index  $\Gamma = 0.9 \pm 0.4$  and a peak energy  $E_p = 72^{+39}_{-6} \text{ keV}$ . The observed burst fluence is  $1.1^{+0.2}_{-0.7} \times 10^{-6} \text{ erg cm}^{-2}$  in the 15–150 keV

band. A fit with a Band model (Band et al. 1993) does not significantly improve the  $\chi^2$  value, albeit this can be due to the low sensitivity of BAT at high energies. Using the best-fit model, we can classify GRB 060927 as an X-ray rich GRB using the definition proposed by Lamb, Donaghy, & Graziani (2005). During the initial prompt emission, hard-to-soft spectral evolution is present, the first spike being significantly harder than the second. The spectrum of the late bump is consistent with that of the second spike.

The X-ray afterglow was detected by XRT about 70 s after the trigger and it was monitored for the following 3 days. The X-ray afterglow position, calculated using the updated boresight (Burrows et al. 2006), is R.A. (J2000) =  $21^{\text{h}}58^{\text{m}}12^{\text{s}}.03$ , decl. (J2000) =  $05^{\circ}21'49''.4$ , with a 90% error radius of  $3''.7$ . This position is within  $0''.7$  of the optical counterpart (§ 2.2). The X-ray light curve displays an initial shallow decay with a slope  $\alpha_1 = 0.71 \pm 0.06$ , steepening to  $\alpha_2 = 1.35 \pm 0.11$  at  $\sim 4 \text{ ks}$  after the trigger. The spectrum is modeled with an absorbed power law with photon index  $\Gamma = 1.87 \pm 0.17$ . After correcting for the Galactic absorption  $N_{\text{H}} = 5.2 \times 10^{20} \text{ cm}^{-2}$ , the 90% confidence limit for the intrinsic absorption is  $N_{\text{H}} < 3.4 \times 10^{20} \text{ cm}^{-2}$  (observer frame). Indeed, little observed X-ray absorption is expected at this large redshift (Grupe et al. 2006; although see GRB 050904: Watson et al. 2006; Cusumano et al. 2006; Campana et al. 2007b), since most of the important absorption edges have been redshifted out of the observed X-ray region. The unabsorbed flux in the 0.3–10 keV energy band from  $T_0 + 75 \text{ s}$  to  $T_0 + 11.3 \text{ ks}$  is  $(5.7 \pm 0.8) \times 10^{-12} \text{ erg cm}^{-2} \text{ s}^{-1}$  from which we derive a lower limit of  $10^{-6} \text{ erg cm}^{-2}$  to the fluence emitted by the X-ray afterglow.

### 2.2. Ground-Based Imaging Observations

The optical afterglow was first detected by the 45 cm telescope of the Robotic Optical Transient Search Experiment in Australia (ROTSE-IIIa). The first unfiltered image started 16.5 s after the burst trigger (Schaefer, Yost, & Yuan 2006), which corresponds to 3 s in the GRB rest frame. Therefore, this is the earliest rest-frame detection of optical emission from any GRB<sup>33</sup>.

Subsequent follow-up observations were obtained by several ground-based facilities. In particular, we used the data from the following instruments: the robotic 2.0 m Faulkes Telescope South (FTS) located at the Siding Spring Observatory, Australia, equipped with RatCam; the 105 cm Schmidt Telescope at the Kiso Observatory in Japan; the 2.56 m Nordic Optical Telescope (NOT), equipped with ALFOSC at La Palma (Canary Islands); the 4.2 m William Herschel Telescope (WHT), using the Aux port imager, also at La Palma; the 1.54 m Danish Telescope situated at La Silla Observatory in Chile; and the 8.2 m Antu and Kueyen Unit Telescopes of the ESO Very Large Telescope (VLT) on Cerro Paranal in Chile, equipped with FORS2 and FORS1, respectively. Near-infrared (NIR) observations were secured using the ISAAC camera on the ESO VLT Antu. In Table 1, we provide the complete observing log. The reduction of the optical and NIR data was performed using standard

<sup>32</sup> <http://heasarc.gsfc.nasa.gov>.

<sup>33</sup> See <http://grad40.as.utexas.edu/grblog.php>.

IRAF<sup>34</sup> tools. The photometry of the afterglow was performed using both PSF-matched and aperture photometry.

Using the VLT image from 2006 September 30, we determined the position of the afterglow to be R.A. (J2000) =  $21^{\text{h}}58^{\text{m}}12^{\text{s}}.02$ , decl. (J2000) =  $+05^{\circ}21'48''.9$ , relative to  $\approx 30$  isolated, non saturated USNO-B1 stars. The estimated uncertainty is about  $0''.2$  in each coordinate.

The detection of the afterglow by ROTSE and the lack of an optical counterpart observation by UVOT on board *Swift* (Oates & Barbier 2006a) revealed within a few minutes that the afterglow of GRB 060927 was very red. This was soon confirmed by the FTS observations, which showed an *I*-band afterglow with no corresponding *R*-band emission within the first 30 minutes after the GRB (Guidorzi et al. 2006a). Later, deep WHT observations taken 8.9 hr after the burst indicated  $R-I > 2.0$ . The *R*-band image from the NOT taken 6.2 hr after the burst reveals a low signal-to-noise detection of the afterglow with  $R \sim 24.4$ . After realizing the high redshift nature of the GRB (see below) we obtained deep *I*-band imaging with the VLT leading to a detection of the afterglow  $\sim 2.6$  days after the burst, and an upper limit at 15 days. We also obtained VLT/ISAAC NIR imaging leading to tentative detections in the *J* and *K* bands. No host galaxy was detected down to  $I > 25.8$  ( $3\sigma$  limit). In Fig. 1 we show the afterglow of GRB 060927 as detected in the ROTSE and *I*-band VLT exposures.

### 2.3. Spectroscopic Observations and Redshift Determination

Spectroscopic observations were performed with the FORS1 instrument at the VLT 12.5 hr after the trigger. We used the grism 300V covering the spectral range from 3600 to 8900 Å at a resolution of 12 Å (using a  $1''.0$  wide slit). The acquisition was performed by aligning the slit with a galaxy  $3''.1$  North of the afterglow and using a position angle for which the slit covered the afterglow position (PA =  $20^{\circ}$  West of North). The afterglow was not detected in the *R*-band acquisition image down to a limiting magnitude  $R \sim 24.0$ .

In the spectrum, a faint continuum is detected at the expected position of the afterglow, but only redward of  $\lambda = 8070$  Å. This feature is similar to what is seen in the spectra of quasars at redshift  $z > 5$  (Cool et al. 2006a). From this clear and sharp discontinuity in the spectrum we conclude that GRB 060927 is a high-redshift event, and is not red because of dust extinction. We interpret the absorption blueward of the break, where the flux level is consistent with zero, as a Ly $\alpha$  forest trough at redshift  $z \approx 5.6$ . In the sky-subtracted two-dimensional spectrum we also clearly detect a single absorption line at  $\lambda = 8148$  Å in a wavelength region clear of bright sky lines (see Fig. 2). This is most likely Si II  $\lambda$  1260 at a redshift of  $z = 5.467$ . At this redshift we would also expect O I/Si II at 1303 Å and C II at 1335 Å, but these fall on bright sky lines and hence would not be detectable. This value for the redshift

supersedes our preliminary determination (Fynbo et al. 2006). The difference in the redshift derived using the hydrogen and silicon lines is due to the presence of strong neutral hydrogen absorption (see § 2.4): the damping wing of the Ly $\alpha$  trough effectively shifts the cutoff at redder wavelengths, mimicking the effect of a larger redshift. In Fig. 2 we show the one-dimensional flux- and wavelength-calibrated spectrum (upper panel) and the processed CCD image (lower panel). In the latter, we can see the sharp continuum break in the afterglow spectrum. The two traces above correspond to nearby objects falling on the slit. We last note that the pseudo-redshift for this burst (Pelangeon & Atteia 2006; Atteia 2003) is  $\hat{z} = 2.37 \pm 0.75$ , significantly different ( $4\sigma$ ) from the spectroscopic value.

### 2.4. Fitting the Red Damping Wing

Measuring the shape of the absorption profile of the damping wing provides a determination of the column density of the neutral hydrogen along the line of sight to the progenitor in the host (Madau & Rees 2000). Using the Fit-Lyman program within MIDAS, we fitted the wing shape with a Damped Ly $\alpha$  absorber system centered at 7861 Å, assuming  $z_{\text{DLA}} = z_{\text{Si II}} = 5.467$ . In Fig. 3 we show the fit to the Ly $\alpha$  and Si II  $\lambda$  1260 absorption line profiles in a  $\pm 30,000$  km s $^{-1}$  velocity interval (solid curve). The best-fit column density is estimated to have  $\log(N_{\text{HI}}/\text{cm}^{-2}) = 22.50 \pm 0.15$ . The  $N_{\text{HI}}$  value is firmly set by the core of the DLA line, i.e., the part of the spectrum which has zero residual flux, whatever the continuum normalisation is. While the error is mostly due to the continuum placement. The  $N_{\text{HI}}$  value is in the range of those found for other *Swift* GRBs at  $z > 2$  (Jakobsson et al. 2006b), although at the high end of the distribution.

## 3. AFTERGLOW PROPERTIES

### 3.1. Light Curve

A major complication with the analysis of the optical light curve is the photometric calibration. The ROTSE data were taken with no filter. For the other telescopes, the *I*-band data were obtained using three different filter variants: an SDSS-like *i* filter for the FTS, the cutoff Harris *I* for the WHT, and the “standard” Bessell *I* for the VLT. For all of them, a significant fraction of the light within the effective filter passband is absorbed by the Ly $\alpha$  forest. This makes it difficult to obtain a meaningful calibrated magnitude or flux from the measured counts.

The ROTSE telescope spectral response is determined by the CCD characteristics, which results in an equivalent broadband filter with a spectral window from 3000 to 10,000 Å and a peak efficiency around 6000 Å. Due to absorption by the Ly $\alpha$  forest, we expect little flux blueward of 8000 Å and therefore our effective response for the optical transient is closer to the *I* band rather than to the *R* band. To obtain a consistently calibrated afterglow flux, we have used the SDSS photometry of neighboring stars (Cool et al. 2006b; Adelman-McCarthy et al. 2006) to establish the numerical conversion factors from ROTSE magnitudes to photon count rates. Six bright, unsaturated and isolated SDSS stars were selected near the GRB for this calibration, spanning a broad range of stellar color. By using the four-band *griz* SDSS data for

<sup>34</sup> IRAF is distributed by the National Optical Astronomy Observatories, which are operated by the Association of Universities for Research in Astronomy, Inc., under cooperative agreement with the National Science Foundation.

these stars, we estimated the total flux in the ROTSE passband. After convolving these total fluxes with the ROTSE spectral response function a model flux for each of the six comparison stars was produced. The RMS variation of these computed values to the ROTSE measurements was 0.09 mag, which gives a reasonable measure of the absolute accuracy of this procedure. We note, however, that since the counterpart was close to detection threshold, statistical uncertainties were always dominating the total error budget.

The next step requires some assumptions about the spectral energy distribution of the GRB afterglow. We adopted a “typical” power-law form,  $F_\nu(\nu) \propto \nu^{-\beta}$ , with  $\beta = 0.75$  (see also § 3.3). This spectrum was folded first with the Ly $\alpha$  absorption in the intergalactic medium (IGM) using the model described by Meiksin (2005) and, second, with the ROTSE spectral response. In the ROTSE passband, 83% of the GRB flux is absorbed by the IGM. Since optical observations must be compared over four different optical passbands, it is desirable to pick a reference wavelength  $\lambda_0$  common to all of them in order to minimize the effects of the uncertainty in  $\beta$ . A sensible choice for  $\lambda_0$  requires it to be higher than the Ly $\alpha$  cutoff frequency (corresponding to 8000 Å) and lower than the long-wavelength cutoff of any of the various *I*-band filters (i.e., 8650 Å for FTS *i*). From the above constraints, we chose arbitrarily  $\lambda_0 = 8190$  Å. Rather than quoting magnitudes based on large extrapolations to actual filter bandwidths, we computed the spectral flux density at the value of  $\lambda_0$  indicated above. We also checked the effect of varying the afterglow spectral index  $\beta$  by  $\pm 0.25$ . Since the observed spectral region is narrowly confined by the Ly $\alpha$  cutoff and by the edge of the filters, the corresponding fluxes are not much changed (by  $\sim 1\%$ ). The inferred flux numerical values are listed in Table 1, and have been corrected for the Galactic extinction  $E(B - V) = 0.06$  mag (Schlegel, Finkbeiner, & Davis 1998) as well.

A similar, but simpler procedure was carried out for the data obtained from the other telescopes. These were in fact equipped with narrow-band filters, so the fraction of light inside the filter lost due to the intergalactic medium absorption was computed. Taking into account the appropriate filter sensitivity functions and the detector quantum efficiencies, this fraction is 68%, 47%, and 56% for the FTS, WHT, and VLT, respectively.

We also note that the afterglow was marginally detected in the *R* band by the NOT and by the Danish 1.54 m telescopes. This detection is very likely due to the extension of the *R*-band filter response redward of 8000 Å. Using the tabulated filter efficiency, we estimate that  $\approx 6\%$  of the light is transmitted (3 mag suppression). Considering the observed color  $R - I = 2.3 \pm 0.3$ , and correcting for the Ly $\alpha$  suppression in both filters, we infer an intrinsic  $R - I = 0.2 \pm 0.3$ , which is consistent with normal afterglow colors given the large uncertainty. We thus confirm that very small light is transmitted blueward of the Ly $\alpha$  cutoff.

In Fig. 4 we present the light curve of the GRB 060927 afterglow, showing *I*-band corrected fluxes and X-ray data points. The X-ray afterglow seems to be rather typical (Zhang et al. 2006; O’Brien et al. 2006; Nousek et al. 2006). At early times ( $t \lesssim 3000$ s) it is characterized by

a shallow decay, with temporal index  $\alpha_1 \approx 0.7$ . Comparison with the extrapolation of the BAT flux also implies a steep decline before the beginning of the observation, showing that GRB 060927 had all the three “canonical” phases. The shallow decline steepened to  $\alpha_2 \approx 1.3$  at  $\sim 4$  ks after the trigger.

The situation is different in the optical. After  $\sim 500$  s the data are fairly well described by a single power law with decay index  $\alpha = 1.17 \pm 0.03$  ( $\chi^2 = 3.6$  with 6 d.o.f.). The early ROTSE data, however, lie significantly below the extrapolation of the late light curve; a single power-law fit to the full *I*-band data set provides an unacceptable  $\chi^2 = 86$  for 11 d.o.f.. A flat light curve between 300 and 1000 s is also visible in the Kiso *R*-band data. The last ROTSE points agree well with the FTS data, so that the difference cannot be due to an intercalibration problem.

One possibility is that a break was present also in the optical, at  $\sim 500$  s after the trigger. Alternatively, the peak at  $\sim 300$  s after the GRB may suggest a rebrightening. The flux after the peak follows a single power law, indicating that no flare was present. Rather, the flux was steadily larger than the extrapolation of the behavior before the brightening. This step-like behavior is consistent with being due to an episode of energy injection. Energy injection is also often invoked to explain the shallow X-ray decay (e.g. Zhang et al. 2006), albeit in GRB 060927 the shallow phase ended significantly later than the brightening episode. A different possibility is that the early emission was due to another component, like a reverse shock or central engine activity (note that the first ROTSE measurements are simultaneous to the last peak of the prompt emission).

It is remarkable that the observed *I*-band flux is declining by the very early observation (3 s in the GRB rest frame). This is difficult to explain in the context of the standard afterglow model (e.g. Sari, Piran, & Narayan 1998). The flux is indeed expected to rise before the so-called deceleration time  $t_{\text{dec}}$ . If the early emission was due to the forward shock, our data constrain  $t_{\text{dec}} \lesssim 3$  s (GRB frame). This translates into a lower limit on the fireball initial Lorentz factor  $\Gamma_0 \gtrsim 1000$ . Furthermore, a break in the light curve is expected when the injection frequency  $\nu_{\text{inj}}$  crosses the observed band. The lack of such a break requires that  $\nu_{\text{inj}}$  was already below the optical range at the beginning of our observations. Very small equipartition parameters are required for this to happen. These difficulties may also support the idea that the early emission was not due to the forward shock.

The optical and X-ray decay slopes at late times are marginally consistent. This is in agreement with the broad-band spectral analysis carried out at  $t \sim 5700$  s (§ 3.3), which shows that the overall SED is well described by a single power law. The hard spectral index  $\beta \approx 0.7$  (Table 2) suggests the cooling frequency was above the X-ray region. However, as discussed before, at early times the X-ray emission was flatter, and the optical light curve showed no steepening at the X-ray break time. This behavior has already been noted in a number of *Swift* bursts (e.g. Panaitescu et al. 2006).

### 3.2. Burst Energetics

The time-averaged spectral energy distribution of the prompt emission is well fitted by a cutoff power law

with a photon index  $\Gamma = 0.9 \pm 0.4$  and a peak energy  $E_p = 72^{+39}_{-6}$  keV. In the burst rest frame, the intrinsic peak energy was  $E'_p = 466^{+250}_{-40}$  keV. The burst fluence over the  $T_{90}$  interval in the 15–150 keV band was  $1.1^{+0.2}_{-0.7} \times 10^{-6}$  erg cm $^{-2}$ . This corresponds to an isotropic-equivalent energy  $E_{\text{iso}} = 7.7^{+2.8}_{-5.0} \times 10^{52}$  erg in the rest-frame 1–10 000 keV band. The values of  $E'_p$  and  $E_{\text{iso}}$  make this GRB consistent with the Amati relation (Amati et al. 2002; Amati 2006).

We can provide only a lower limit to any light curve break, which corresponds to  $t_b \gtrsim 2.6$  days (the epoch of our last detection). The lower limits for the jet opening angle and for the beaming-corrected energy are  $\vartheta > 5^\circ$  and  $E_{\text{jet}} > 2.6 \times 10^{50}$  erg, respectively. The  $E'_p$  vs  $E_{\text{jet}}$  correlation (Ghirlanda et al. 2004) predicts for this burst  $t_b = 10^{+8}_{-4}$  days (Campana et al. 2007b), thus GRB 060927 is consistent with this relation, although it does not constrain it (see also Ghirlanda et al. 2007).

### 3.3. The Afterglow Spectral Energy Distribution

We have constructed the spectral energy distribution (SED) of the afterglow covering from NIR to X-ray wavelengths at 5709 s after the *Swift* BAT trigger. Both a power law (PL) and a broken power law (BPL) have been fitted including the effect of dust absorption, adopting the extinction curves of the Milky Way (MW), the Large Magellanic Cloud (LMC) and the Small Magellanic Cloud (SMC) as parametrized by Pei (1992), and of photoelectric absorption in the X-ray band (assuming Solar metallicity). All fits include a fixed Galactic absorption component, with  $N_{\text{H,Gal}} = 5.2 \times 10^{20}$  cm $^{-2}$  (Dickey & Lockman 1990) and  $E(B - V) = 0.062$  mag. Correction for Ly $\alpha$  blanketing was applied to the  $I$  and  $R$  data. When excluding the  $R$  band data, which are severely suppressed, the parameters did not change within the errors. All the results are listed in Table 2, and the best fit is shown in Fig. 5. Also considering the broad-band SED, we do not measure any intrinsic X-ray absorption, consistent with the XRT analysis alone. A broken power law with photon indices  $\Gamma_1$  and  $\Gamma_2$  provides no improvement upon the single power law fits, and the break energies are difficult to constrain. We also test for the presence of a cooling break in the observed energy range by fixing  $\Gamma_1 = \Gamma_2 - 0.5$ , as expected from the standard synchrotron theory, but found that no such break is required. The optical absorption is found to be low, in agreement with many previous studies of GRB host galaxy extinction (e.g., Kann et al. 2006; Starling et al. 2007). However, it is not possible in this case to differentiate between the three tested extinction curves. The 2175 Å bump characteristic of the MW extinction curve would occur at  $\sim 1.4 \mu\text{m}$  when redshifted to  $z = 5.47$ , falling in between the  $J$  and  $K$  bands where we have no observations. From our data we can, however, obtain an accurate measurement of the power-law slope at this epoch, which is consistent within the errors with the value derived from fitting the X-ray data alone (§ 2.1). The similar decay indices in the optical and X-ray ranges also suggests that both components lie on the same spectral segment.

## 4. GAMMA-RAY BURSTS AS PROBES OF THE DARK AGES

Spectroscopy of GRB afterglows has been argued to be a powerful tool to probe the red Ly $\alpha$  damping wing resulting from the neutral intergalactic medium before reionization (Barkana & Loeb 2004). In fact, they have simple power-law continuum spectra and a relatively small ionizing effect on their environments (compared to QSOs). This shape allows one to directly infer the neutral hydrogen column and hence the state of reionization (Madau & Rees 2000). However, as pointed out by Totani et al. (2006), this method may be compromised by the strong hydrogen absorption due to the dense environments that long GRBs usually seem to be situated in (Jakobsson et al. 2006b). Our observation that such a high absorbing column is also present in a  $z > 5$  GRB confirms that it is likely difficult to use afterglow spectra as a diagnostic of reionization due to the Ly $\alpha$  damping wing. We also note, however, that GRB-DLA column densities are usually lower than for GRB 060927: in the sample by Jakobsson et al. (2006b) only two out of 18 events ( $\approx 10\%$ ) have  $N_{\text{HI}} > 10^{22.5}$  cm $^{-2}$ . Furthermore, as pointed out by (Bromm & Loeb 2007), it is conceivable that higher-redshift bursts may explode inside less massive halos, and thus with lower column densities.

The outlook for the use of GRBs as star-formation tracers is much better. For example, it has also been suggested by Wijers et al. (1998) that GRBs could be *ideal* tracers of the average star formation density due to their brightness, independently of dust extinction and the fact that they originate from a single (or double) stellar progenitor and so do not require a detectable host galaxy (see also Conselice et al. 2005). Evidence has been mounting that GRBs may only trace star formation in relatively metal-poor environments (e.g. Le Floc'h et al. 2003; Fynbo et al. 2003; Tanvir et al. 2004; Sollerman et al. 2005; Fruchter et al. 2006; Stanek et al. 2006; Modjaz et al. 2007). In the popular collapsar model, GRBs are expected to be formed only by stars with metallicity below about  $0.2\text{--}0.3Z_\odot$  (Heger et al. 2003; MacFadyen & Woosley 1999; Hirschi, Meynet, & Maeder 2005; Woosley & Heger 2006; Langer & Norman 2006, but see also Fryer & Heger 2005). However, before  $z \approx 5$  the majority of the star-formation should occur in environments with  $Z < 0.2Z_\odot$  (Nuza et al. 2007), and therefore the redshift distribution of  $z > 5$  GRBs should directly map the star formation history of the universe back to the first era of population-II objects, and possibly the first population-III stars (e.g. Bromm & Loeb 2006; Belczynski et al. 2007).

Furthermore, GRBs afterglows pinpoint their host galaxies, provide redshifts for them, and in some cases measures of their metallicity, gas density and dynamical state<sup>35</sup>. This provides a route to identify and study the types of galaxies that are responsible for the bulk of the star formation, and hence for the bulk of the (re-)ionization of the universe. This is very important since other methods to locate high redshift galaxies with current instrumentation only locate the brightest systems

<sup>35</sup> Although the existence of the GRB might select environments with special properties, recent observations (Chen et al. 2007; Watson et al. 2007; Vreeswijk et al. 2007) have shown that the material being probed by afterglow spectroscopy is not in the immediate surroundings of the GRB site, implying that it may be representative of the host galaxy properties.

that are too rare to account for the bulk of the ionization (Labbé et al. 2006), possibly with the exception of gravitational lensing (Stark et al. 2007).

*Swift* has been operating for more than two years and we now have a good sample of GRBs from which to constrain their fraction at very high redshift. We followed Jakobsson et al. (2006a) and selected only *Swift* GRBs with low Galactic extinction and promptly determined XRT positions. In this way we created an unbiased sample with a larger redshift completeness, discarding those bursts with adverse observing conditions. By December 2006, there had been a total of 83 of these bursts: 46 with spectroscopic redshift measurements (with a mean  $\langle z \rangle = 2.31$ ), 18 with no optical/NIR afterglow nor host galaxy detection, and 19 with optical/NIR afterglow or host galaxy detection but unknown spectroscopic redshift. In order to compile this list, we browsed the literature, and we also made use of the preliminary results of an ongoing large program aimed at detecting GRB host galaxies and measuring their redshifts (J. Hjorth et al. 2007 in preparation; Jakobsson et al. (2006c)). In Fig. 6 we show the redshift distribution for the 83 bursts. The arrows indicate upper limits based on the information available: afterglow colors, host galaxy and/or Ly $\alpha$  break constraints. The shaded bar indicates bursts for which we have no redshift information at all.

Several bursts in the sample with very red afterglows have shown properties expected for high-redshift bursts: GRB 050502B, GRB 050716, GRB 060108, GRB 060602A, GRB 060719, GRB 060814, GRB 060923A and GRB 060923C (Cenko et al. 2005; Tanvir et al. 2005; Levan, Tanvir, & Fuhrman 2006a; Jensen et al. 2006; Malesani et al. 2006; Levan et al. 2006b; Fox, Rau, & Ofek 2006; D’Avanzo et al. 2006, respectively). However, for GRB 060108 (Oates et al. 2006b), GRB 060814 (Campana et al. 2007c), and GRB 060923A (Levan, Tanvir, & Gorosabel 2006c), the detection of the host galaxy in the  $R$  band indicates  $z \lesssim 5.5$  and hence the red afterglow color is due to dust extinction rather than to high redshift<sup>36</sup>.

We now try to constrain the fraction  $f$  of *Swift* GRBs at  $z > 6$ . From the initial sample we removed bursts with measured or constrained redshift, leading to a subsample of 20 candidates: 18 bursts with no information at all and 2 bursts with very loose redshift constraints. We rejected from this set those bursts with duration shorter than 14 seconds<sup>37</sup> and those with (significant) excess column density in the X-ray spectra. As pointed out by Grupe et al. (2006), high-redshift GRBs tend to show little or no X-ray absorption, since the affected spectral region is redshifted out of the observing window (see however the striking counterexample of GRB 050904 at  $z = 6.295$ : Watson et al. 2006; Cusumano et al. 2006; Campana et al. 2007b). Only six bursts were considered as candidates for being at  $z > 6$ . Together with GRB 050904, they set an upper limit of  $f < 7/83 \approx 8\%$ . Do we have any evidence that these bursts are at high redshift? We retrieved from the literature optical magnitude upper lim-

its<sup>38</sup> and X-ray fluxes<sup>39</sup> (Butler & Kocevski 2007) in order to estimate an upper limit to the optical-to-X-ray spectral index  $\beta_{\text{OX}}$ . High-redshift bursts necessarily have  $\beta_{\text{OX}} < 0.5$  (Jakobsson et al. 2004). Unfortunately, the existing observational limits are not deep enough to constrain  $\beta_{\text{OX}} < 0.5$  for any of the candidates. By considering GRB 050904, we can thus set a lower limit  $f \gtrsim 1/83 \approx 1\%$ , even if we caution, of course, that this limit is based on one single event. It has been argued (Butler & Kocevski 2007) that afterglow spectra may be intrinsically curved (due to the presence of spectral breaks) and this could spuriously mimic the presence of excess column density. If we remove the requirement of zero excess absorption, the upper limit on  $f$  becomes  $f < 16/83 \approx 19\%$ , which is of course less constraining and very conservative.

From what is shown above, it is possible that *Swift* had detected some GRBs with  $z > 6$  in addition to GRB 050904. How do we improve our follow-up strategies in order to identify these bursts and secure spectroscopic redshifts? It is clear from the discussion above that the afterglows of such events will be very red due to Lyman-forest blanketing, but that not all red afterglows are from high redshift bursts. Fortunately, the dust-extinguished bursts will likely be behind large column densities of soft X-ray absorbing material and hence can be filtered away (Grupe et al. 2006). The main issue is therefore to detect the NIR afterglows.

The two most distant GRBs known, GRB 050904 (e.g. Kawai et al. 2006; Haislip et al. 2006; Gendre et al. 2006; Totani et al. 2006; Tagliaferri et al. 2005) and GRB 060927 (this work), were both detected with relatively small aperture robotic telescopes (TAROT and ROTSE-IIIa, respectively). This suggests that we may expect bright afterglows from a substantial fraction of GRBs with  $z > 6$ , but these will not be detectable with most of the currently operating robotic instruments because of the lack of light in the optical window. NIR robotic projects (e.g. REM, GROND on the ESO 2.2m, the 1.3m CTIO telescope, PAIRITEL, BOOTES-IR) are expected to provide accurate afterglow positions in just a few minutes, and, hence, to increase the sample of spectroscopically measured high-redshift GRBs. However, three of these are placed within a few hundred kilometers of each other in Chile. In order to make the search of events that are only visible in the NIR as efficient as in the optical, a more wide-spread net of NIR (semi-)robotic telescopes is required. A possible solution, easy to implement on a short time scale, is to equip many of the 1.5–3 m class telescopes, that have had less observing demands since the advent of 8–10 m telescopes, with red-sensitive deep-depletion CCDs and  $z$ -band filters (see e.g. Guidorzi et al. 2006b). In this way the probability of detecting bursts out to  $z \approx 7.5$  would dramatically increase.

## 5. SUMMARY AND CONCLUSIONS

We have presented X-ray and optical observations of the afterglow of GRB 060927, performed with the *Swift* spacecraft and several ground-based telescopes. The spectroscopic observations made with the VLT showed

<sup>36</sup> The afterglow of GRB 060108 was also detected in the  $B$  band, implying a low redshift  $z < 3.2$  (Oates et al. 2006b).

<sup>37</sup> A burst with  $T_{90} = 14$  s at  $z = 6$  has a proper time duration of  $\approx 2$  s; see also Campana et al. (2007c).

<sup>38</sup> <http://grad40.as.utexas.edu/grblog.php>.

<sup>39</sup> <http://astro.berkeley.edu/~nat/swift>.

a flux dropout starting at  $\lambda = 8070 \text{ \AA}$ . We interpret the absorption blueward of the break as due to the Ly $\alpha$  forest at redshift  $z \approx 5.6$ . We also detect a Si II  $\lambda 1260$  absorption line at  $\lambda = 8148 \text{ \AA}$ , corresponding to  $z = 5.467$ .

The modeling of the red damping wing of the Ly $\alpha$  absorption found in the optical afterglow spectrum leads to a column density with  $\log(N_{\text{HI}}/\text{cm}^{-2}) = 22.50 \pm 0.15$ . This is similar to the values observed in GRBs at lower redshift. Such large values make the use of the GRBs to probe the reionization epoch via spectroscopy of the red damping wing challenging.

The light curve in the gamma-ray band shows an initial bright episode, split in two peaks, with a total duration  $T_{90} = 22.6 \pm 0.3 \text{ s}$ . The X-ray light curve is characterized by a shallow decline phase lasting  $\sim 3000 \text{ s}$ , with the temporal index being  $\alpha_1 \approx 0.7$ . The shallow decline steepened to  $\alpha_2 \approx 1.3$  at  $\sim 4 \text{ ks}$  after the trigger. The optical data are fairly well described by a single power law with decay index  $\alpha = 1.17 \pm 0.03$  after  $\sim 500 \text{ s}$ , while an extra component is apparent at earlier times.

We selected a sample of *Swift* GRBs with low Galactic extinction and promptly determined XRT positions. From this unbiased sample, we constrain the fraction  $f$  of GRBs at  $z > 6$ . Including GRB 050904, we set a conservative upper limit  $f < 19\%$ . We also point out that GRB 060927 was detected by a 45 cm telescope

(ROTSE). This shows that high-redshift GRBs can be very bright, and are in principle easy to detect, provided that red and near-infrared detectors are employed. We suggest to exploit the potential of the  $z$ -band filter, capable to detect bursts up to  $z \approx 7.5$ .

The Dark Cosmology Centre is funded by the Danish National Research Foundation. The authors acknowledge benefits from collaboration within the EU FP5 Research Training Network “Gamma-Ray Bursts: An Enigma and a Tool”. DM acknowledges financial support from the Instrument Center for Danish Astrophysics. JG acknowledges the support of Spanish research programmes ESP2005-07714-C03-03 and AYA2004-01515. PJ acknowledges support by a Marie Curie Intra-European Fellowship within the 6th European Community Framework Program under contract number MEIF-CT-2006-042001. ROTSE-III has been supported by NASA grant NNG-04WC41G, NSF grant AST-0407061, the Australian Research Council, the University of New South Wales, the University of Texas, and the University of Michigan. Work performed at LANL is supported through internal LDRD funding. Special thanks to the observatory staff at Paranal and Siding Spring Observatory, especially Andre Phillips.

#### REFERENCES

- Adelman-McCarthy, J. K., et al. 2006, *ApJS*, 162, 38  
 Amati, L., et al. 2002, *A&A*, 390, 81  
 Amati, L. 2006, *MNRAS*, 372, 233  
 Atteia, J.-L. 2003, *A&A*, 407, L1  
 Band, D., et al. 1993, *ApJ*, 413, 281  
 Band, D. L. 2006, *ApJ*, 644, 378  
 Barkana, R., & Loeb, A. 2004, *ApJ*, 601, 64  
 Belczynski, K., Bulik, T., Heger, A., & Fryer, C. 2007, *ApJ*, in press (astro-ph/0610014)  
 Bromm, L., & Loeb, A. 2006, *ApJ*, 642, 382  
 Bromm, L., & Loeb, A. 2007, review to appear in “Gamma-ray Bursts” (CUP) (arXiv:0706.2445)  
 Burrows, D. N., Moretti, A., Perri, M., Capalbi, M., Angelini, L., & Hill, J. E. 2006, *GCN* 5750  
 Butler, N. R., & Kocevski, D. 2007, *ApJ*, 663, 407  
 Campana, S., et al. 2007a, *ApJ*, 654, L17  
 Campana, S., Guidorzi, C., Tagliaferri, G., Chincarini, G., Moretti, A., Rizzuto, D., & Romano, P. 2007b, *A&A*, in press (astro-ph/0703676)  
 Campana, S., Tagliaferri, G., Malesani, D., Stella, L., D’Avanzo, P., Chincarini, G., & Covino, S. 2007c, *A&A*, 464, L25  
 Cenko, S. B., Fox, D. B., Rich, J., Schmidt, B., Christiansen, J., & Berger, E. 2005, *GCN Circular* 3358  
 Chen, H.-W., Prochaska, J. X., Ramirez-Ruiz, E., Bloom, J. S., Dessauges-Zavadsky, M., & Foley, R. 2007, *ApJ*, 663, 420  
 Conselice, C. J., et al. 2005, *ApJ*, 633, 29  
 Cool, R. J., et al. 2006a, *AJ*, 132, 823  
 Cool, R. J., et al. 2006b, *GCN Circular* 5631  
 Cusumano, G., et al. 2006, *Nature*, 440, 164  
 D’Avanzo, P., Covino, S., Malesani, D., & Tagliaferri, G. 2006, *GCN Circular* 5609  
 Dickey, J. M., & Lockman, F. J. 1990, *ARA&A*, 28, 215  
 Fox, D. B., Rau, A., & Ofek, E. O. 2006, *GCN Circular* 5597  
 Fruchter, A. S., et al. 2006, *Nature*, 441, 463  
 Fryer, C. L., & Heger, A. 2005, *ApJ*, 623, 302  
 Fynbo, J. P. U., et al. 2003, *A&A*, 406, L63  
 Fynbo, J. P. U., et al. 2006, *GCN Circular* 5651  
 Galama, T. J., et al. 1998, *Nature*, 395, 670  
 Gehrels, N., et al. 2004, *ApJ*, 611, 1005  
 Gendre, B., Galli, A., Corsi, A., Klotz, A., Piro, L., Stratta, G., Boër, M., & Damerdjian, Y. 2006, *A&A*, 462, 565  
 Ghirlanda, G., Ghisellini, G., & Lazzati, D. 2004, *ApJ*, 616, 331  
 Ghirlanda, G., Nava, L., Ghisellini, G., & Firmani, C. 2007, *A&A*, 466, 127  
 Grupe, D., et al. 2006, *AJ*, 133, 2216  
 Guidorzi, C., et al. 2006, *GCN Circular* 5633  
 Guidorzi, C., et al. 2006, *PASP*, 118, 288  
 Haislip, J. B., et al. 2006, *Nature*, 440, 181  
 Heger, A., Fryer, C. L., Woosley, S. E., Langer, N., & Hartmann, D. H. 2003, *ApJ*, 591, 288  
 Hirschi, R., Meynet, G., & Maeder, A. 2005, *A&A*, 443, 581  
 Hjorth, J., et al. 2003, *Nature*, 423, 847  
 Jakobsson, P., Hjorth, J., Fynbo, J. P. U., Watson, D., Pedersen, K., Björnsson, G., & Gorosabel, J. 2004, *ApJ*, 617, L21  
 Jakobsson, P., et al. 2006a, *A&A*, 447, 897  
 Jakobsson, P., et al. 2006b, *A&A*, 460, L13  
 Jakobsson, P., Hjorth, J., Fynbo, J. P. U., Gorosabel, J., & Jaunsen, A. O. 2006c, *procs. of the XI Marcel Grossman Meeting on General Relativity*, eds. H. Kleinert, R. T. Jantzen, & R. Ruffini (astro-ph/0611561)  
 Jensen, B. L., Hjorth, J., Fynbo, J. P. U., & Näränen, J. 2006, *GCN Circular* 5203  
 Kann, D. A., Zeh, A., & Klose, S. 2006, *ApJ*, 641, 993  
 Kawai, N., et al. 2006, *Nature*, 440, 184  
 Kouveliotou, C., Meegan, C. A., Fishman, G. J., Bhat, N. P., Briggs, M. S., Koshut, T. M., Paciesas, W. S., & Pendleton, G. N. 1993, *ApJ*, 413, L101  
 Labbé, I., Bowens, R., Illingworth, G. D., & Franx, M. 2006, *ApJ*, 649, L67  
 Lamb, D. Q., & Reichart, D. E. 2000, *ApJ*, 536, 1  
 Lamb, D. Q., Donaghy, T. Q., & Graziani, C. 2005, *ApJ*, 620, 355  
 Le Floc’h, E., et al. 2003, *A&A*, 400, 499  
 Levan, A. J., Tanvir, N. R., & Fuhrman, L. 2006a, *GCN Circular* 4503  
 Levan, A. J., Tanvir, N. R., Rol, E., Fruchter, A., & Adamson, A. 2006b, *GCN Circular* 5455  
 Levan, A. J., Tanvir, N. R., & Gorosabel, J. 2006c, *GCN Circular* 5673  
 MacFadyen, A. I., & Woosley, S. E. 1999, *ApJ*, 524, 262  
 Madau, P., & Rees, M. J. 2000, *ApJ*, 542, L69  
 Malesani, D., Fynbo, J., D’Avanzo, P., Covino, S., Fugazza, D., Jakobsson, P., & Vreeswijk, P. M. 2006, *GCN Circular* 5354  
 Meiksin, A. 2005, *MNRAS*, 356, 596  
 Modjaz, M., et al. 2007, *AJ*, submitted (astro-ph/0701246)  
 Langer, N., & Norman, C. A. 2006, *ApJ*, 638, L63  
 Nousek J. A., et al. 2006, *ApJ*, 642, 389  
 Nuza, S. E., Tissera, P. B., Pellizza, J., Lambas, D. G., Scannapieco, C., & De Rossi, M. E. 2007, *MNRAS*, 375, 665

- Oates, S. R., & Barbier, L. M. 2006, GCN Circular 5643
- Oates, S. R., et al. 2006, MNRAS, 372, 327
- O’Brien, P. T., et al. 2006, New J. Phys., 8, 121
- Panaiteanu, A., Mészáros, P., Burrows, D., Nousek, J., Gehrels, N., O’Brien, P., & Willingale, R. 2006, MNRAS, 369, 2059
- Pei Y. C. 1992, ApJ, 395, 130
- Pelangeon, A., & Atteia, J.-L. 2006, GCN Circular 5644
- Sari, R., Piran, T., & Narayan, R. 1998, ApJ, 497, L17
- Schaefer, B. E., Yost, S. A., & Yuan, F. 2006, GCN Circular 5629
- Schlegel, D. J., Finkbeiner, D. P., & Davis, M. 1998, ApJ, 500, 525
- Sollerman, J., Östlin, G., Fynbo, J. P. U., Hjorth, J., Fruchter, A., & Pedersen, K. 2005, New Astr. 11, 103
- Stanek, K. Z., et al. 2003, ApJ, 591, L17
- Stanek, K. Z., et al. 2006, Acta Astronomica, 56, 333
- Stark, D. P., et al. 2007, ApJ, 663, 10
- Starling, R. L. C., Wijers, R. A. M. J., Wiersema, K., Rol, E., Curran, P. A., Kouveliotou, C., van der Horst, A. J., & Heemskerk, M. H. M. 2007, ApJ, 661, 787
- Tagliaferri, G., et al. 2005, A&A, 443, L1
- Tanvir N. R., et al. 2004, MNRAS, 352, 1073
- Tanvir, N., et al. 2005, GCN Circular 3632
- Totani, T., Kawai, N., Kosugi, G., Aoki, K., Yamada, T., Iye, M., Ohta, K., & Hattori, T. 2006, PASJ, 58, 485
- Vreeswijk, P. M., et al. 2007, A&A, 468, 83
- Watson, D., et al. 2006, ApJ, 637, L69
- Watson, D., Hjorth, J., Fynbo, J. P. U., Jakobsson, P., Foley, S., Sollerman, J., & Wijers, R. A. M. J. 2007, ApJ, 660, L101
- Wijers, R. A. M. J., Bloom, J. S., Bagla, J. S., & Natarajan, P. 1998, MNRAS, 294, L13
- Woosley, S. E., & Heger, A. 2006, ApJ, 637, 914
- Zhang, B., Fan, Y. Z., Dyks, J., Kobayashi, S., Mészáros, P., Burrows, D. N., Nousek, J. A., & Gehrels, N. 2006, ApJ, 642, 354



TABLE 1  
GROUND-BASED OBSERVATIONS OF GRB 060927. UPPER LIMITS ARE AT THE  $3\sigma$  LEVEL.

Time (UT) <sup>a</sup>	$\Delta t$ (s)	Exposure (s)	Magnitude <sup>b</sup>	$F_\nu(\lambda_0)^c$	Filter	Telescope
Sep. 27.588794	16.8	5	14.39 $\pm$ 0.20	6800 $\pm$ 1300	none	0.45-m ROTSE-IIIa
Sep. 27.588956	30.8	5	14.67 $\pm$ 0.22	5200 $\pm$ 1100	none	0.45-m ROTSE-IIIa
Sep. 27.589216	53.3	15	15.56 $\pm$ 0.19	2290 $\pm$ 410	none	0.45-m ROTSE-IIIa
Sep. 27.589804	104.1	25	17.16 $\pm$ 0.41	520 $\pm$ 200	none	0.45-m ROTSE-IIIa
Sep. 27.590624	174.9	200	17.86 $\pm$ 0.30	275 $\pm$ 78	none	0.45-m ROTSE-IIIa
Sep. 27.594007	467.2	600	17.07 $\pm$ 0.21	570 $\pm$ 110	none	0.45-m ROTSE-IIIa
Sep. 27.602126	1168.7	600	17.99 $\pm$ 0.40	243 $\pm$ 92	none	0.45-m ROTSE-IIIa
Sep. 27.654894	5727.9	600	> 17.04	< 590	none	0.45-m ROTSE-IIIa
Sep. 27.593845	453.2	930	> 20.1	...	SDSS <i>R</i>	2.0-m FTS
Sep. 27.597834	797.9	60	> 18.4	< 570	SDSS <i>i</i>	2.0-m FTS
Sep. 27.602725	1221.3	120	19.02 $\pm$ 0.17	320 $\pm$ 50	SDSS <i>i</i>	2.0-m FTS
Sep. 27.609716	1824.4	180	19.64 $\pm$ 0.22	180 $\pm$ 37	SDSS <i>i</i>	2.0-m FTS
Sep. 27.616009	2368.2	120	19.43 $\pm$ 0.27	220 $\pm$ 55	SDSS <i>i</i>	2.0-m FTS
Sep. 27.623009	2973.0	180	20.57 $\pm$ 0.47	77 $\pm$ 33	SDSS <i>i</i>	2.0-m FTS
Sep. 27.602650	1214.0	90	19.5 $\pm$ 0.3	...	<i>R</i>	1.05-m Kiso
Sep. 27.627431	3355.0	90	19.4 $\pm$ 0.1	...	<i>R</i>	1.05-m Kiso
Sep. 27.629468	3531.0	90	19.8 $\pm$ 0.2	...	<i>R</i>	1.05-m Kiso
Sep. 27.844120	$2.21 \times 10^4$	$3 \times 300$	24.4 $\pm$ 0.3	...	<i>R</i>	2.5-m NOT
Sep. 27.957326	$3.18 \times 10^4$	$4 \times 100$	> 25.5	...	<i>B</i>	4.2-m WHT
Sep. 27.964109	$3.24 \times 10^4$	$4 \times 100$	> 24.6	...	<i>V</i>	4.2-m WHT
Sep. 27.973495	$3.32 \times 10^4$	$4 \times 100$	> 24.2	...	<i>R</i>	4.2-m WHT
Sep. 27.978808	$3.37 \times 10^4$	$4 \times 100$	22.11 $\pm$ 0.16	7.2 $\pm$ 1.1	Harris <i>I</i>	4.2-m WHT
Sep. 28.006500	$3.61 \times 10^4$	$13 \times 900$	24.5 $\pm$ 0.26	...	Bessell <i>R</i>	1.54-m Danish
Sep. 28.064850	$4.11 \times 10^4$	$2 \times 60$	>24.0	...	Bessell <i>R</i>	8.2-m VLT
Sep. 28.108681	$4.49 \times 10^4$	$3 \times 1800$	...	...	G300V	8.2-m VLT
Sep. 30.004618	$2.09 \times 10^5$	$10 \times 30$	21.35 $\pm$ 0.29	...	<i>K</i>	8.2-m VLT
Sep. 30.039178	$2.12 \times 10^5$	$30 \times 60$	23.15 $\pm$ 0.45	...	<i>J</i>	8.2-m VLT
Sep. 30.159225	$2.22 \times 10^5$	$21 \times 300$	24.85 $\pm$ 0.17	0.72 $\pm$ 0.11	Bessell <i>I</i>	8.2-m VLT
Oct. 13.067980	$1.34 \times 10^6$	$25 \times 300$	> 25.8	< 0.3	Bessell <i>I</i>	8.2-m VLT

<sup>a</sup> The reported times correspond to the beginning of the observation.

<sup>b</sup> Not corrected for Galactic extinction.

<sup>c</sup> Flux density at  $\lambda_0 = 8190$  Å, measured in  $\mu\text{Jy}$ , corrected for Galactic extinction  $E(B - V) = 0.06$  mag.

TABLE 2  
MODEL FITS TO THE SED AT EPOCH 5709 s SINCE TRIGGER. ALL ERRORS ARE AT THE 90% CONFIDENCE LEVEL.

Model <sup>a</sup>	Ext. curve <sup>b</sup>	$N_H$ <sup>c</sup>	$E(B - V)$	$\Gamma_1$	$E_b$ (keV)	$\Gamma_2$	$\chi^2/\text{dof}$
PL	MW	< 1.2	0.13 $^{+0.03}_{-0.02}$	1.70 $\pm$ 0.06	...	...	9.5/20
PL	MW	0 (frozen)	0.13 $^{+0.06}_{-0.05}$	1.70 $\pm$ 0.06	...	...	9.5/21
PL	LMC	< 1.1	0.08 $^{+0.02}_{-0.01}$	1.68 $^{+0.04}_{-0.06}$	...	...	10.7/20
PL	LMC	0 (frozen)	0.08 $^{+0.04}_{-0.03}$	1.68 $^{+0.05}_{-0.06}$	...	...	10.7/21
PL	SMC	< 1.0	0.07 $^{+0.01}_{-0.02}$	1.61 $^{+0.05}_{-0.04}$	...	...	11.5/20
PL	SMC	0 (frozen)	0.07 $\pm$ 0.03	1.66 $^{+0.10}_{-0.05}$	...	...	11.5/21
BPL	MW	< 3.6	0.11 $^{+0.06}_{-0.07}$	1.64 $^{+0.09}_{-0.21}$	<106	1.83 $^{+7.17}_{-0}$	6.6/18
BPL ( $\Gamma_1 = \Gamma_2 - 0.5$ )	MW	< 4.7	0.13 $^{+0.06}_{-0.09}$	>1.0	>1.0	2.19 $^{+0.06}_{-0.13}$	8.9/19
BPL	LMC	< 3.6	0.07 $\pm$ 0.04	1.63 $^{+0.07}_{-0.21}$	<2.7	1.83 $^{+0.33}_{-0}$	7.0/18
BPL ( $\Gamma_1 = \Gamma_2 - 0.5$ )	LMC	< 4.8	0.07 $^{+0.05}_{-0.04}$	>0.9	>0.9	2.13 $^{+0.09}_{-0.08}$	9.5/19
BPL	SMC	< 3.5	0.05 $^{+0.04}_{-0.03}$	1.66 $^{+0.07}_{-0.21}$	<2.4	1.83 $^{+0.31}_{-0}$	7.0/18
BPL ( $\Gamma_1 = \Gamma_2 - 0.5$ )	SMC	< 4.8	0.05 $^{+0.04}_{-0.03}$	>0.8	>0.8	2.12 $^{+0.07}_{-0.08}$	9.5/19

<sup>a</sup> PL: power law with photon index  $\Gamma_1$ ; BPL: broken power law with photon indices  $\Gamma_1, \Gamma_2$  and break energy  $E_b$ .

<sup>b</sup> MW: Milky Way; LMC: Large Magellanic Cloud; SMC: Small Magellanic Cloud.

<sup>c</sup> Rest-frame hydrogen column density in units of  $10^{22} \text{ cm}^{-2}$ .

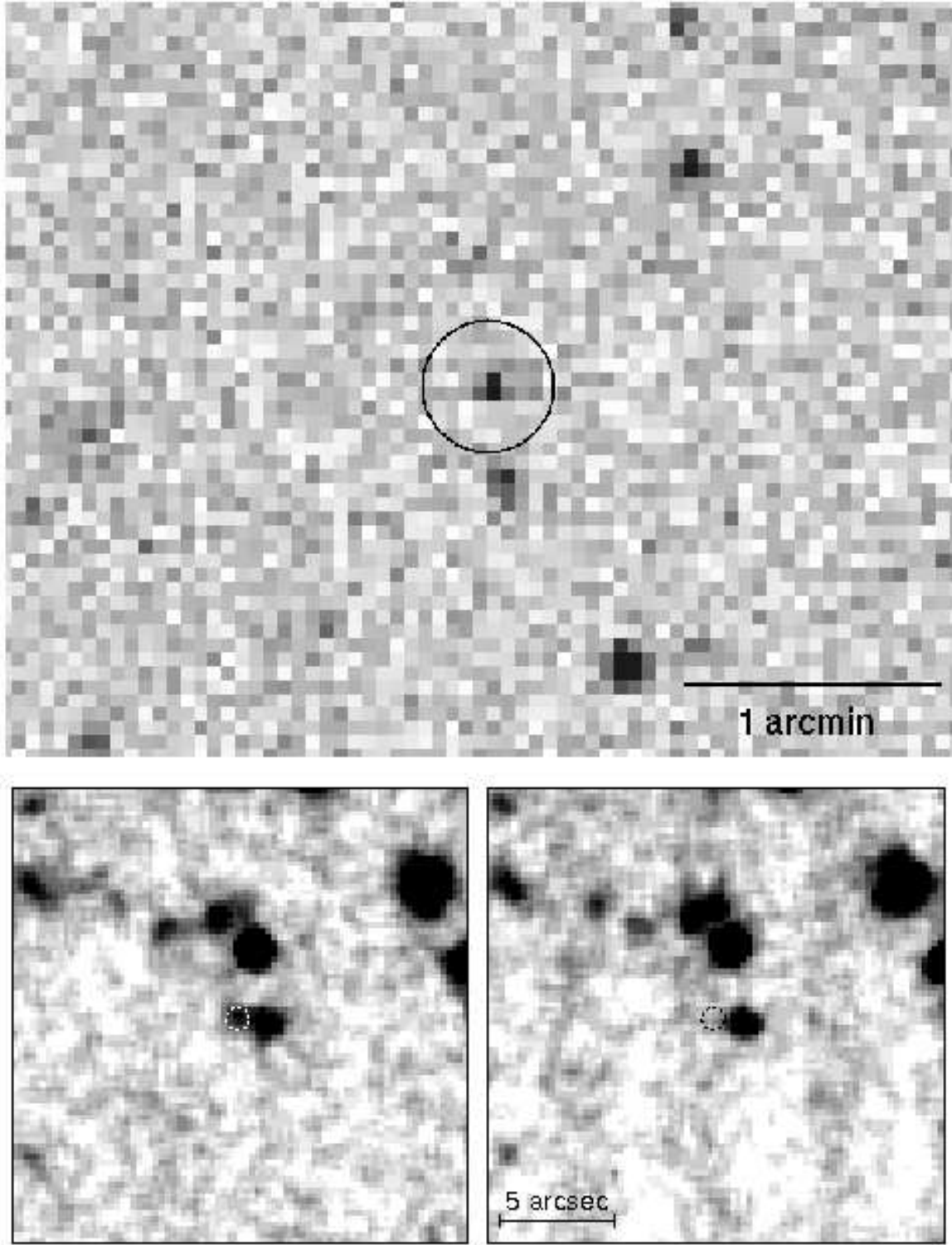


FIG. 1.— Top: unfiltered image from ROTSE-IIIa obtained 19 s after the trigger. Bottom: VLT *I*-band images 2.6 days (left) and 15.5 days (right) after the trigger. The circles indicate the position of the optical afterglow. North is up, East is left.

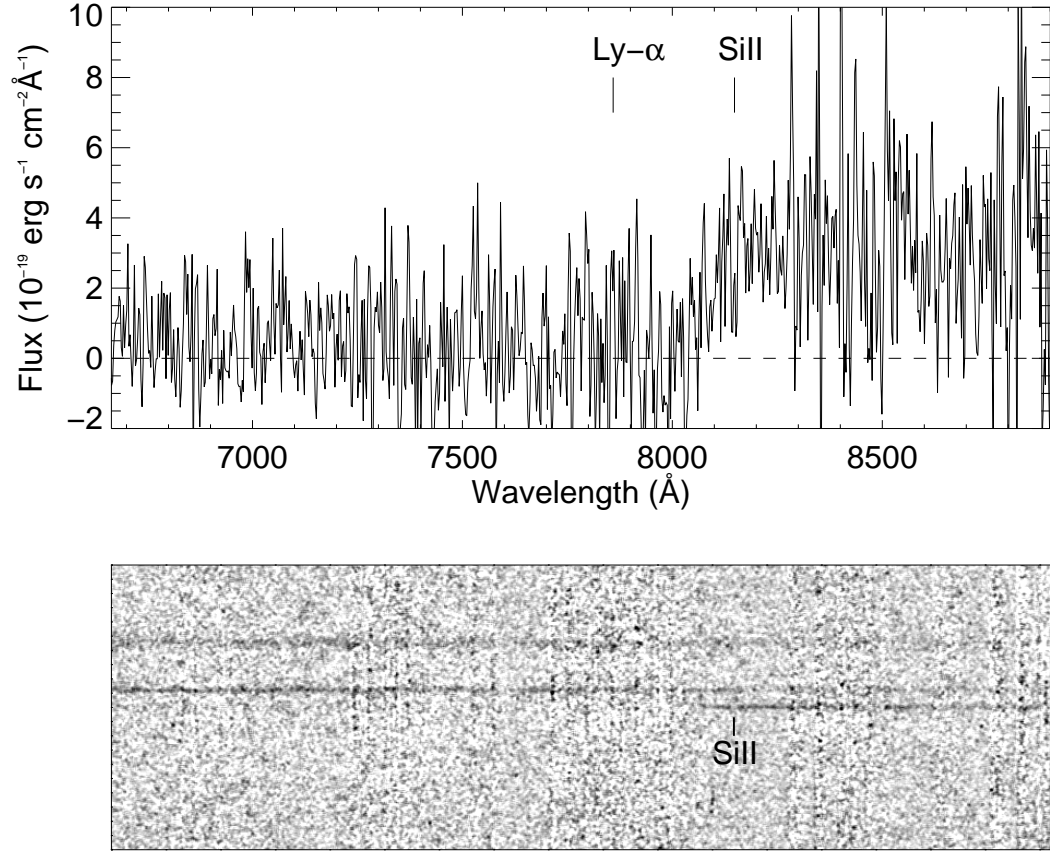


FIG. 2.— Afterglow spectrum of GRB 060927 taken 12.5 hr after the trigger. The one-dimensional spectrum is shown in the upper panel with the identified absorption Ly $\alpha$  and Si II lines indicated. The CCD image of the spectrum in the corresponding wavelength range is shown in the lower panel (bottom trace).

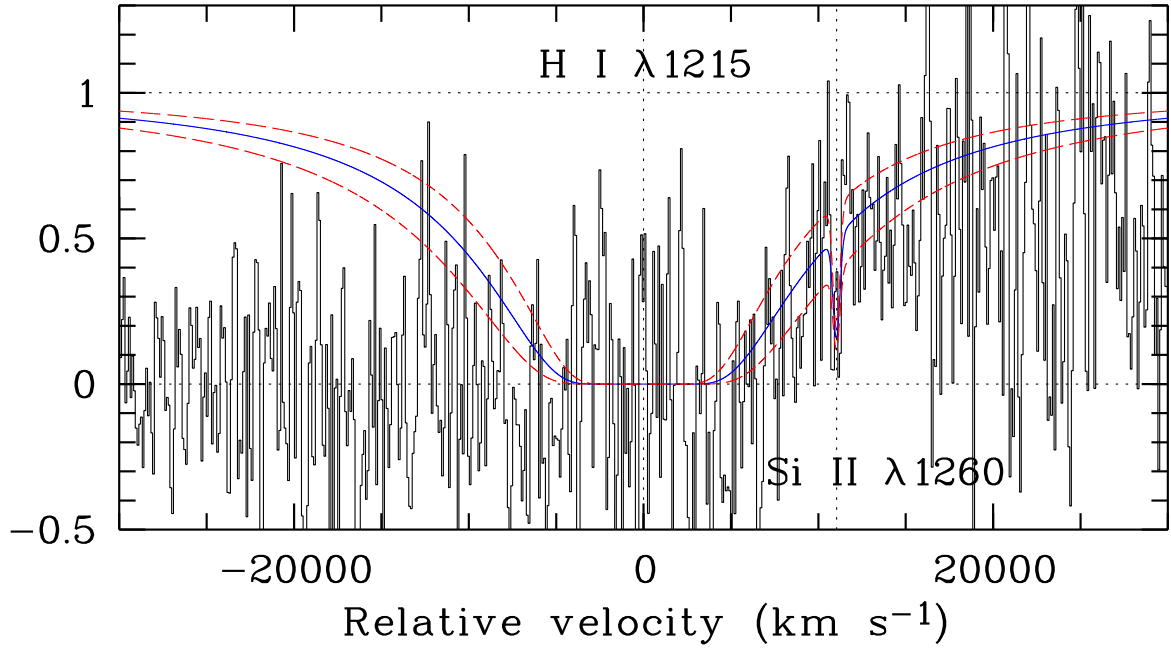


FIG. 3.— Afterglow spectrum with the model fit to the Ly $\alpha$  and Si II  $\lambda$  1260 absorption line profiles (solid curve). The corresponding column density has  $\log(N_{\text{HI}}/\text{cm}^{-2}) = 22.50 \pm 0.15$ .

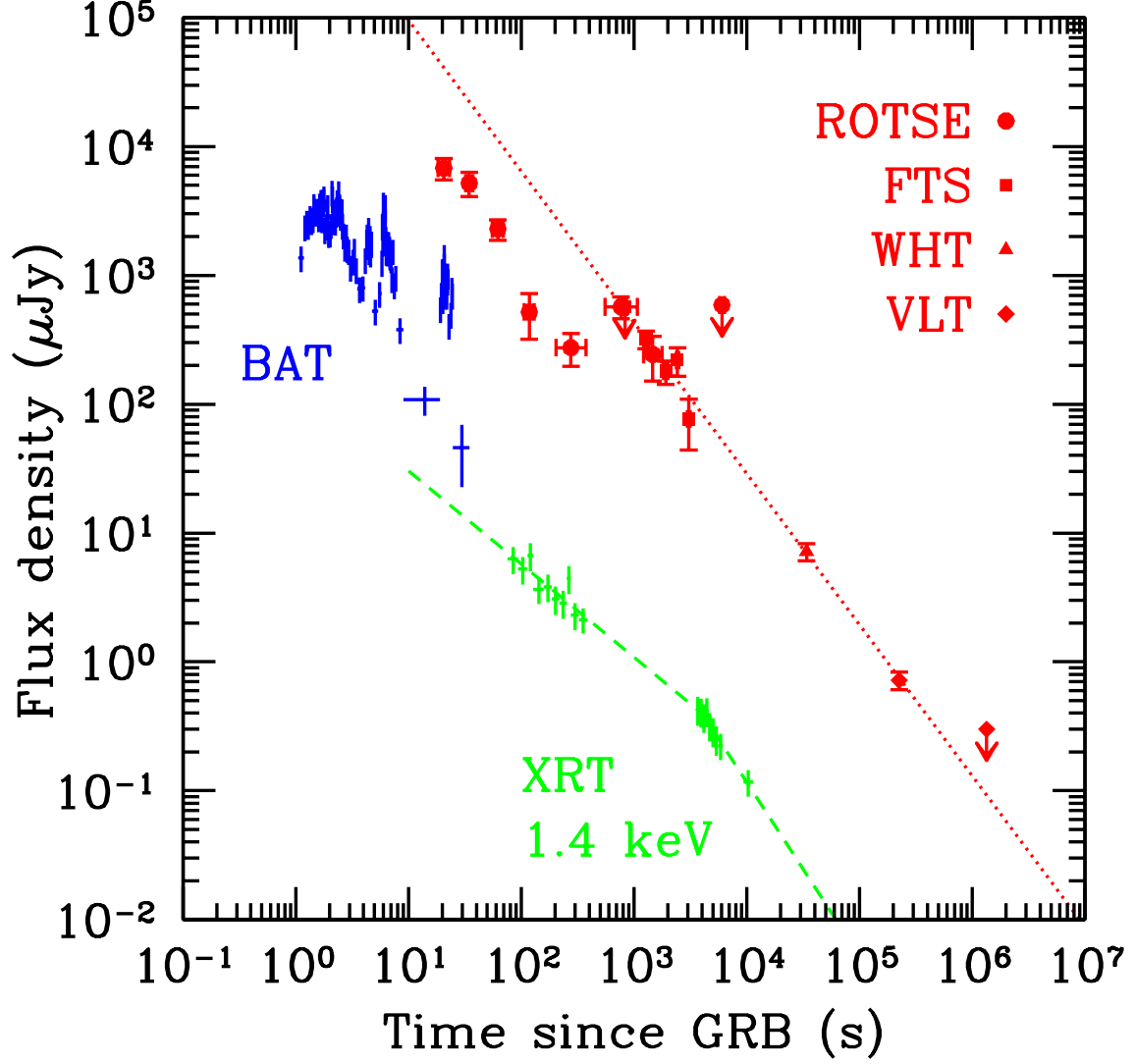


FIG. 4.— Optical (8190 Å, filled symbols) and X-ray (1.4 keV, crosses) light curves of GRB 060927. The early BAT measurements were extrapolated to the XRT range using the best-fit spectral model. Optical data were corrected for the Galactic extinction. The dotted line shows the best-fit power-law model to the  $I$ -band light curve for  $t > 500$  s, while the dashed line shows the best-fit broken power-law model to the X-ray light curve.

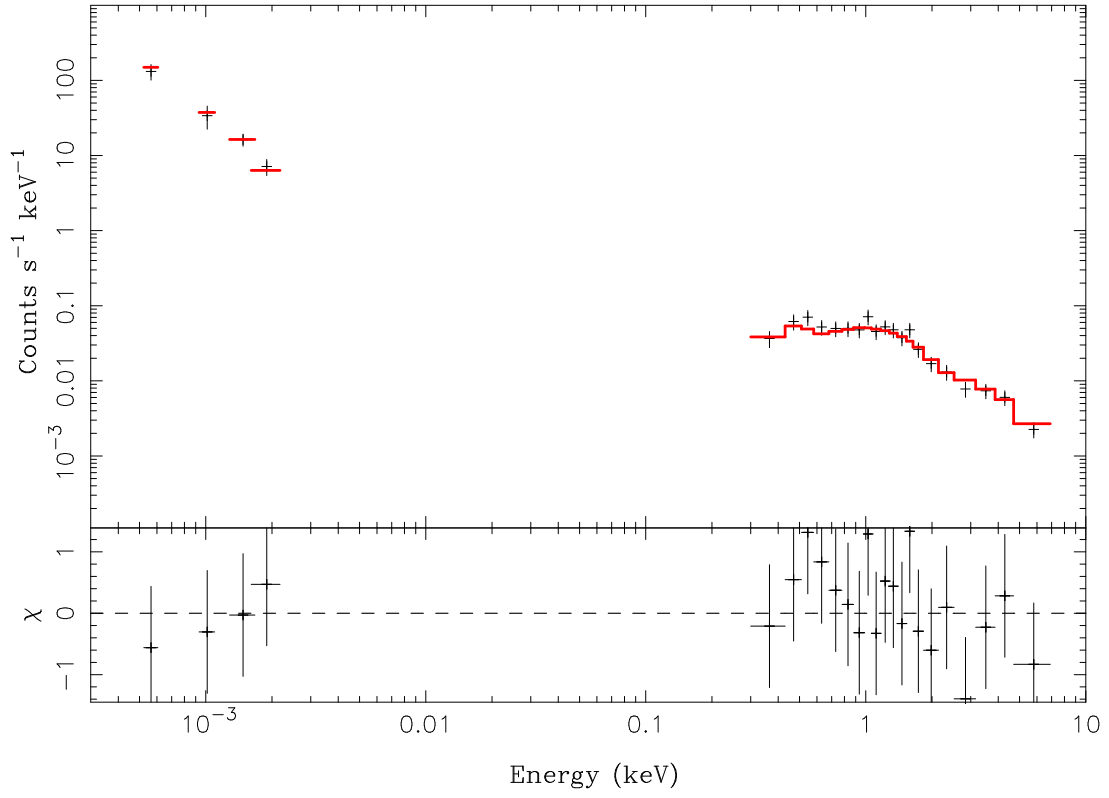


FIG. 5.— Example of fit to the NIR/X-ray SED. The model (thick solid line) shows a single power law with Milky-Way extinction. The lower panel shows the residuals of the fit.

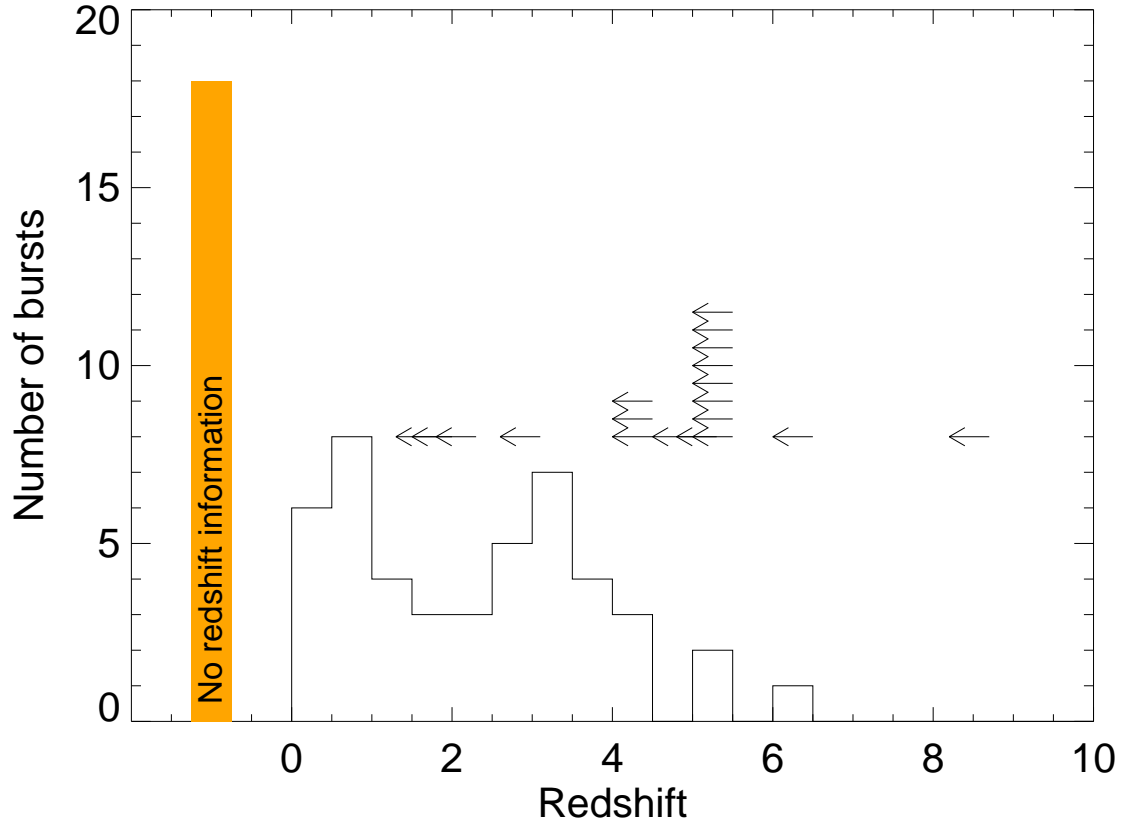


FIG. 6.— The redshift distribution of *Swift* GRBs up to 2006 December. The arrows indicate upper limits based on the afterglow colors and/or presence of Ly $\alpha$  breaks in the spectra and/or detection of the host galaxy. The shaded bar indicates the 18 bursts for which we have no constraints on the redshift.